Conformation and Lipid Binding of the N-Terminal (1−44) Domain of Human Apolipoprotein A-I[†]

Hongli L. Zhu and David Atkinson*

Department of Physiology and Biophysics, Boston University School of Medicine, 715 Albany Street, Boston, Massachusetts 02118

Received June 10, 2004; Revised Manuscript Received July 20, 2004

ABSTRACT: Because of its role in reverse cholesterol transport, human apolipoprotein A-I is the most widely studied exchangeable apolipoprotein. Residues 1−43 of human apoA-I, encoded by exon 3 of the gene, are highly conserved and less well understood than residues 44−243, encoded by exon 4. In contrast to residues 44−243, residues 1−43 do not contain the 22 amino acid tandem repeats thought to form lipid binding amphipathic helices. To understand the structural and functional roles of the N-terminal region, we studied a synthetic peptide representing the first 44 residues of human apoA-I ([1−44]apoA-I). Far-ultraviolet circular dichroism spectra showed that [1−44]apoA-I is unfolded in aqueous solution. However, in the presence of *n*-octyl β-D-glucopyranoside, a nonionic lipid mimicking detergent, above its critical micelle concentration (∼0.7% at 25 °C), sodium dodecyl sulfate, an ionic detergent, above its CMC (∼0.2%), trimethylamine *N*-oxide, a folding inducing organic osmolyte, or trifluoroethanol, an α-helix inducer, α-helical structure was formed in [1−44]apoA-I up to ∼45%. Characterization by density gradient ultracentrifugation and visualization by negative staining electron microscopy demonstrated that [1−44]apoA-I interacts with dimyristoylphosphatidylcholine (DMPC) over a wide range of lipid:peptide ratios from 1:1 to 12:1 (w/w). At 1:1 DMPC:[1−44]apoA-I (w/w) ratio, discoidal complexes with composition ∼4:1 (w/w) and ∼100 Å diameter were formed in equilibrium with free peptide. At higher ratios, discoidal complexes were shown to exist together with a heterogeneous population of lipid vesicles with peptide bound also in equilibrium with free peptide. When bound to DMPC, [1−44]apoA-I has ∼60% helical structure, independent of whether it forms discoidal or vesicular complexes. This helical content is consistent with that of the predicted G* helix (residues 8−33). Our data provide the first strong and direct evidence that the N-terminal region of apoA-I binds lipid and can form discoidal structures and a heterogeneous population of vesicles. In doing so, ∼60% of this region folds into α-helix from random coil. The composition of the 100 Å discoidal complex is ∼5 [1−44]apoA-I and ∼150 DMPC molecules per disk. The helix length of 5 [1−44]apoA-I molecules in lipid-bound form is just long enough to wrap around the DMPC bilayer disk once.

Coronary artery disease is the number one cause of death in the United States and other parts in the world. High-density lipoproteins (HDL)[1] and human apolipoprotein A-I (apoA-I, A-I, 243 amino acids) have been studied extensively over the past 30 years because HDL is anti-atherogenic (*1*, *2*) and apoA-I is the major protein component of HDL. The mechanisms of the anti-atherogenic effect of HDL are mainly related to its involvement in the pathways of reverse cholesterol transport (RCT) (*3*). ApoA-I participates in the entire RCT pathway through interaction with three other important proteins. It interacts with ABC-A1 that mediates the efflux of phospholipids and cholesterol from cells in peripheral tissue. It is the cofactor of the enzyme LCAT that converts cholesterol into cholesterol ester and results in the nascent discoidal HDL to mature spherical HDL transformation. It is the ligand for the SR-BI receptor that is responsible for SR-BI-mediated cholesterol ester uptake by the liver (*4*, *5*).

In the gene, the first 43 residues of apoA-I are encoded by exon 3, and the rest of the molecule is encoded by exon 4. The sequence of apoA-I contains 10 (H1−H10) tandem 11 or 22 amino acid residue repeats thought to form lipid binding amphipathic helices that are defined by the exon 4 encoded region (*6*). Sequence analysis (*7*), crystal structure determination of Δ(1−43) apoA-I (*8*), and NMR assignments (*9*, *10*) have provided different helix distributions with different flexible regions and different helical positions. Segment deletion and point mutations have been studied to elucidate the possible function for each helical segment. Both N- and C-terminal regions are important for lipid association and cholesterol esterification (*11*). Residues 121−164

[†] This work was supported by Grant POHL26335 from the National Institutes of Health.

* To whom correspondence should be addressed. Phone: (617) 638-4015. Fax: (617) 638-4041. E-mail: Atkinson@bu.edu.

[1] Abbreviations: apoA-I/A-I, human apolipoprotein A-I; ABC-A1, ATP binding cassette A1; BOG, *n*-octyl β-D-glucopyranoside; far-UV CD, far-ultraviolet circular dichroism; CMC, critical micelle concentration; DMPC, dimyristoylphosphatidylcholine; EM, electron microscopy; HDL, high-density lipoprotein; LCAT, lecithin:cholesterol acyltransferase; NMR, nuclear magnetic resonance; [1−44]apoA-I, residues 1−44 of human apoA-I; PK, peak fraction; RCT, reverse cholesterol transport; SDS, sodium dodecyl sulfate; TFE, trifluoroethanol; TMAO, trimethylamine *N*-oxide.

10.1021/bi0487894 CCC: $27.50
Published on Web 09/25/2004

(H5/H6) show the lowest lipid binding affinity and are required for LCAT activation (*12*−*15*), whereas the C-terminal domain is required for interaction with ABC-A1 (*16*).

In contrast to the exon 4 encoded region, the first 43 residues are less understood. The sequence of this N-terminal region is highly conserved among mammalian species (*17*). However, it contains the most ambiguously defined structure and was deleted in the only available crystal structure of apoA-I at 4 Å resolution (*8*) because of its flexibility. On the basis of sequence analysis, three antiparallel β-strands were predicted from residue 14 to residue 57 by Nolte and Atkinson (*7*). Later, a G* helix was predicted from residue 8 to residue 33 (*18*). Recent NMR assignment data suggest a helix from residue 8 to residue 32 in SDS solution (*9*, *10*). The function of this N-terminal domain is not clear. Initially, it was thought to be a non-lipid binding region (*19*). However, a synthetic peptide representing the first 33 residues showed lipid binding affinity (*20*). There is no direct evidence that the N-terminal domain of apoA-I plays a specific role in the anti-atherogenic function of apoA-I. However, several studies have suggested that the N-terminal domain is close to and interacts with the C-terminal domain (*21*−*23*) and thus may stabilize the apoA-I conformation important for anti-atherogenic function.

A major feature of apoA-I is conformational flexibility that allows the structure to adapt to a lipid-free environment and the different lipid environments of nascent discoidal HDL and spherical HDL. The lack of a defined apoA-I tertiary structure can be explained by the low cooperativity [$\Delta H_v(T_m)/\Delta H(T_m) \sim 0.16$] of the thermal unfolding of lipid-free apoA-I and the small free energy of stabilization ($\Delta G \sim 2.4$ kcal/mol) (*24*). This inherent flexibility has precluded crystallographic and other studies of the structural details. Lipid-free apoA-I may exist in an α-helix bundle conformation. In nascent discoidal HDL, apoA-I wraps around a phospholipid bilayer. In spherical HDL, with a cholesterol ester core, apoA-I interacts with the phospholipid monolayer at the spherical surface. Among the three conformations, the nascent discoidal HDL has been a focus of study. Understanding apoA-I secondary structure and conformational adaptability is key to understanding apoA-I function.

Since apoA-I adopts dynamic conformations depending on different lipid association states, the extreme N-terminal domain may undergo secondary structural changes in different lipid association states. In this study, we report a conformational characterization and the lipid interactions of the N-terminal 44 residues ([1−44]apoA-I).

MATERIALS AND METHODS

Peptide Synthesis. [1−44]ApoA-I, amidated at the C-terminus, was synthesized by Quality Controlled Biochemicals, Inc. (Hopkinton, MA) at a purity of >95%. The purity of the peptide was further verified by mass spectroscopy. The experimentally determined molecular weight was 4934, consistent with the calculated molecular weight from the amino acid sequence of 4937 for amidated [1−44]apoA-I.

Chemicals. n-Octyl β-D-glucopyranoside (BOG) was purchased from Dojindo Laboratories (Dojindo Molecular Technologies, Inc., Gaithersburg, MD). Trifluoroethanol (TFE) was purchased from Aldrich Chemical Co. (Milwaukee, WI). Trimethylamine *N*-oxide (TMAO), sodium dodecyl sulfate (SDS), and dimyristoylphosphatidylcholine (DMPC) were from Sigma (St. Louis, MO). [^{14}C]DPPC ([*dipalmitoyl*-1-^{14}C]-L-α-dipalmitoylphosphatidylcholine, 110.00 mCi/mmol, 0.05 mCi/mL) was from New England Nuclear (now PerkinElmer Life and Analytical Sciences, Inc., Boston, MA). All chemicals used were of analytical grade purity. All solutions were made from doubly distilled water and were filtered by 0.2 μm Millipore filters.

Peptide Concentration. The concentrations of peptide and peptide in BOG/TMAO/SDS were determined by Lowry assay (*25*). For lipid-containing samples such as DMPC/[1−44]apoA-I mixtures, the assay was modified slightly. Samples were treated as usual in the Lowry assay. After final color development, 2 mL of chloroform was added. The sample was vortexed and spun at 2000 rpm at 15 °C for 15 min. The aqueous layer was transferred to the cuvette for concentration determination.

Circular Dichroism (CD) Spectroscopy. Far-UV CD spectra were recorded using an AVIV 62 DS spectropolarimeter. The wavelength CD spectra were recorded from 250 to 190 or 185 nm at 25 °C, with a 1 nm step size and 15 s accumulation time per data point, and averaged over at least three consecutive scans. Melting curves were recorded from 5 to 95 °C at 222 nm (the negative CD band of an α-helix), with a 1.00 °C step size, 40−300 s accumulation time per data point, and zero equilibration time. Buffer baselines were subtracted from the data that were normalized to the peptide concentration and expressed as molar ellipticity. Protein α-helical content was determined with 3% accuracy from the molar residue ellipticity at 222 nm, $[\theta]_{222}$, according to (*26*)

$$\% \alpha = \frac{[\theta]_{222} + 3000}{36000 + 3000} \times 100$$

Sample Preparation and Data Collection. Freshly dissolved peptide in 10 mM phosphate buffer at pH 7.0 was used in all of the experiments. BOG/TMAO/SDS were freshly dissolved in phosphate buffer and then diluted to the required concentrations. TFE was diluted to the required concentration directly. Peptide concentration was kept consistent at ∼0.1 mg/mL for all CD experiments unless specified.

Peptide−DMPC mixtures were made by spontaneous association of the peptide with a turbid suspension of DMPC liposomes at room temperature in phosphate buffer. A wide range of initial DMPC:[1−44]apoA-I ratios from 1:1 to 12:1 (w/w) were studied. It took from several minutes to ∼24 h for the liposome suspension to clear depending on the lipid:peptide ratio. Lower ratios cleared more rapidly. After the solution became clear, it was used for CD experiments and EM visualization.

Preparation and Density Gradient Analysis of the [1−44]ApoA-I/DMPC Interaction. The interaction of [1−44]apoA-I with DMPC was carried out at various initial DMPC:[1−44]apoA-I (w/w) ratios from 1:1 to 12:1, keeping DMPC constant at 1 mg. To quantitate the lipid, 5 μL of [^{14}C]DPPC (DPPC:DMPC ∼1:13000 M) was added to 4 mL of ∼5 mg/mL DMPC dissolved in $CHCl_3$ (accurate concentration determined by dry weight per 10 μL volume just before mixing). Because $CHCl_3$ readily evaporates, the

concentration of the labeled DMPC was determined each time just before use. One milligram of DMPC (volume required by the concentration) was aliquoted in a 20 mL glass vial and dried on the lyophilizer under nitrogen. It was further dried in a desiccator overnight at 4 °C. Varying amounts of phosphate buffer (pH 7.0), as required by the DMPC:[1−44]apoA-I (w/w) ratio, were added. Vigorous vortexing was required to make liposomes from the dried DMPC. Various amounts of [1−44]apoA-I, as required by the ratios, were added individually. The total volume for each sample was 1 mL. One milliliter of PBS was added to the DMPC control vial and a blank control vial.

The density of the samples and the blank was adjusted to ∼1.2 g/mL using solid KBr, and the samples were transferred to 5 mL SW-55 ultraclear tubes. All of the samples were overlaid with 1.065 g/mL KBr. The tubes were spun at 50K rpm, 15 °C, for 48 h. Preliminary experiments, carried out for 24 and 48 h, determined that 48 h was required for the gradients to reach equilibrium. After spinning, 25 aliquots of 200 mL each were pipetted from the surface of the solution. To determine the density, the refractive index of each fraction of the blank was measured on a Leica Abbe Mark I refractometer. For each fraction, peptide was determined by modified Lowry assay, and lipid was determined by [^{14}C]DPPC scintillation counting.

Electron Microscopy. [1−44]ApoA-I−DMPC complexes, simple mixtures and peak fractions after density gradient separation, were visualized by electron microscopy using the negative staining technique (*27*). Samples were observed on a CM12 electron microscope (Philips Electron Optics, Eindhoven, The Netherlands). Representative fields were photographed with an exposure time of 1.00 s, at 45× magnification.

Calculation of Discoildal Complex Compostions. According to the diameter of the discoidal complex from EM visualization, the number of DMPC per disk was estimated from

$$\text{no. of DMPC per disk} = 2\pi[(d - 20)/2]^2/70$$

(We assume a helix diameter of 10 Å and a surface area/DMPC of 70 Å^2. The unit of d is angstroms.)

The molar ratio of lipid:peptide for each fraction was determined from the lipid/peptide mass distribution in the density gradient.

RESULTS

Conformational Characterization of [1−44]ApoA-I in Solution by Circular Dichroism. (A) [1−44]ApoA-I in Aqueous Solution. Figure 1A shows far-UV CD spectra of [1−44]apoA-I over a concentration range of 0.05−0.5 mg/mL. The overall spectrum, with a minimum at 200 nm, indicates that [1−44]apoA-I is unstructured over this concentration range. α-Helical content, calculated from θ_{222} (25 °C), is ∼15%, which is the typical for random coil structure. There is no apparent β-sheet contribution. In contrast to apoA-I that self-associates above 0.1 mg/mL, [1−44]apoA-I does not self-associate even at concentrations up to 0.5 mg/mL, because the CD spectrum is unchanged over the 10-fold concentration range. Lack of self-association was confirmed by cross-linking with glutaraldehyde and SDS gradient gel electrophoresis (data not shown).

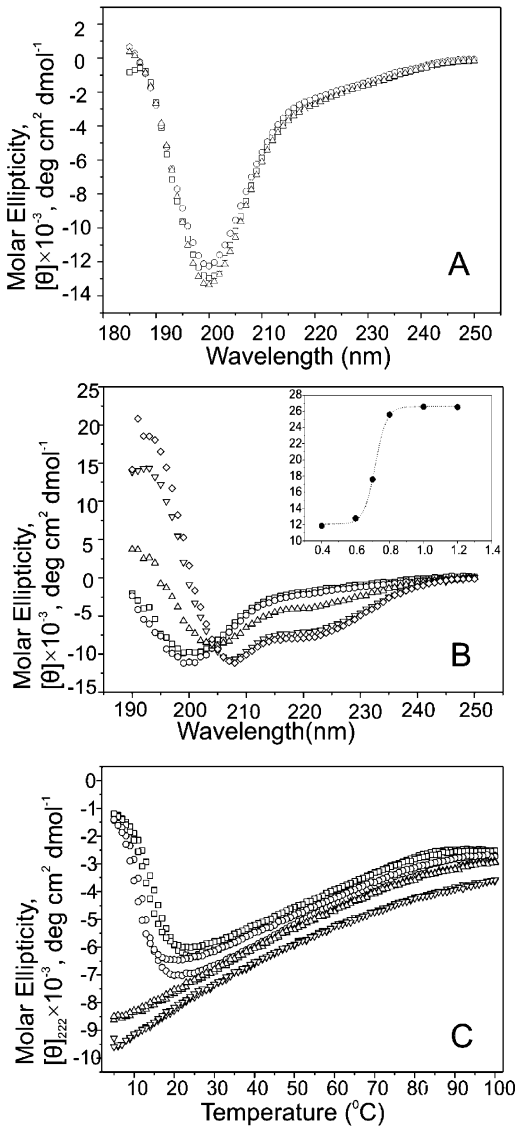

FIGURE 1: (A) Far-UV CD spectra of [1−44]apoA-I at pH 7.0 and 25 °C: (○) 0.05 mg/mL, (△) 0.1 mg/mL, and (□) 0.5 mg/mL. The samples were in 0.01 M phosphate. (B) Far-UV CD spectra of [1−44]apoA-I in different [BOG]: (□) 0.4%, (○) 0.6%, (△) 0.7%, (▽) 0.8%, and (◇) 3.0%. The insert figure is the α-helical percentage of [1−44]apoA-I on the basis of θ_{222} as a function of [BOG]. (C) Thermal unfolding of [1−44]apoA-I as a function of [BOG] monitored by CD at 222 nm: (□) 0.8%, (○) 0.9%, (△) 1.2%, and (▽) 3.0%. The samples contained 0.1 mg/mL [1−44]-apoA-I and 0.01 M phosphate.

(B) [1−44]ApoA-I in BOG Solution. BOG is a small, nonionic lipid-mimicking detergent. Figure 1B shows far-UV CD spectra of [1−44]apoA-I at various BOG concentrations below and above the CMC (0.7%) at 25 °C. Below the CMC, there is little effect on the CD spectrum that remains indicative of random coil. At and above 0.7% (CMC), the spectrum shows pronounced minima at 208 and 222 nm, typical of α-helix. The insert to Figure 1B shows the α-helical content of [1−44]apoA-I as a function of BOG concentration. The maximum α-helical content is ∼27% in 3.0% BOG at 25 °C. The helical structure of [1−44]apoA-I in BOG increases in a sigmoidal manner, indicating that the formation of helical structure is concomitant to the formation of BOG micelles.

The melting of the helical structure in [1−44]apoA-I, as measured by θ_{222}, at four concentrations of BOG from 0.8%

Table 1: Helical Content of [1−44]ApoA-I in Variant Agents

[BOG] (w/v) (%)	% α-helix[a]	[SDS] (w/v) (%)	% α-helix[a]	[TMAO] (M)	% α-helix[a]	[TFE] (v/v) (%)	% α-helix[a]
0	13	0	15	0	15	0	14
0.7	18	0.05	24	2	30	10	18
0.8	23	0.1	36	3	31	20	35
1.0	27	0.2	41	4	39	30	36
1.2	27	0.4	42	6	38	60	44
3.0	28	1.6	42			80	45

[a] The α-helical content is the mean value at 25 °C, derived from three to five independent measurements of two to three different samples. The error in this estimate is 3%.

to 3.0% is shown in Figure 1C and exhibits characteristics similar to that of segment 99−142 of human apoA-I [corresponding to helix repeat 5 and 6 (*28*)]. Each sample was heated from 5 to 95 °C and cooled directly from 95 to 5 °C. Different melting rates, from 40 s/point to 3 min/point, showed no significant differences. Wavelength scans at 25 °C, recorded immediately before and after melting, were unchanged. Thus heating and cooling do not affect [1−44]-apoA-I concentration, and the thermal unfolding is reversible. In the presence of the higher BOG concentrations (1.2% and 3.0%), the far-UV CD signal of [1−44]apoA-I at 222 nm increases continuously as the temperature increases from 5 to 95 °C, whereas in lower BOG concentrations (0.8% and 0.9%), the far-UV CD signal of [1−44]apoA-I first decreases as the temperature increases from 5 to ∼20 °C and then increases continuously as the temperature increases from ∼20 to 95 °C. The far-UV CD signal at 222 nm for [1−44]-apoA-I in 0.9% BOG starts to increase 2 °C before that of [1−44]apoA-I in 0.8% BOG.

(C) [1−44]ApoA-I in SDS, TMAO, and TFE Solution. In SDS, an ionic detergent, and two common protein folding reagents, TMAO and TFE, varying amounts of helical structure were induced in [1−44]apoA-I (Table 1). SDS has a molecular weight similar to that of BOG and forms micelles over a more broad concentration range from 0.1% to 2%. [1−44]ApoA-I in SDS showed far-UV CD spectral changes similar to those in BOG (data not shown). Interestingly, [1−44]apoA-I gained more helical content, up to ∼45%, in SDS. This is ∼15% more than the maximum in BOG. TMAO, a protein structure inducer, was used to test what kinds of secondary components could exist in the peptide. Far-UV CD spectra of [1−44]apoA-I in the presence of TMAO over a concentration range from 2 to 6 M exhibited typical helical characteristics (spectra not shown). The maximum helical content was ∼40%. TFE, a helical structure inducer, was used to examine the maximum helical content that could be induced. In ≥60% (v/v) TFE, the helical content reached a maximum of ∼45%. Thermal unfolding and refolding of [1−44]apoA-I in SDS/TMAO/TFE were also reversible.

Lipid Binding of [1−44]ApoA-I: Density Gradient Ultracentrifugation and EM. Figure 2A shows the far-UV CD spectra of [1−44]apoA-I in various amounts of DMPC at 25 °C. Eight initial ratios of DMPC:[1−44]apoA-I [1:1, 2:1, 3:1, 4:1, 6:1, 7.5:1, 9:1, and 12:1 (w/w)] were examined. Similar to the observations in BOG and SDS, [1−44]apoA-I in DMPC folds into α-helix in a DMPC concentration dependent manner and reaches an apparent

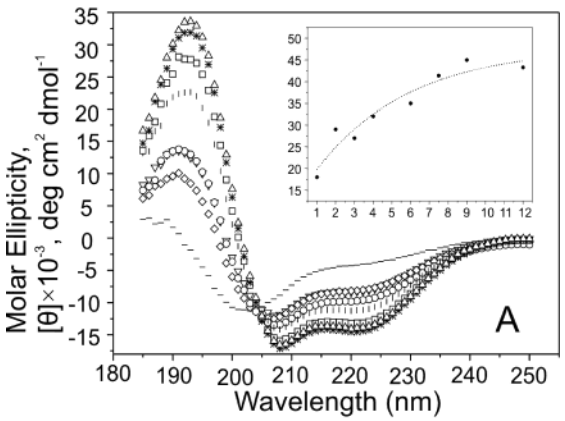

Simple mixture of DMPC:[1-44]apoA-I w:w 6:1

FIGURE 2: (A) Far-UV CD spectra of [1−44]apoA-I/DMPC simple mixtures at different DMPC:[1−44]apoA-I (w/w) ratios at pH 7.0 and 25 °C: (EnDash−) 1:1, (▽) 2:1, (◇) 3:1, (○) 4:1, (|) 6:1, (□) 7.5:1, (△) 9:1, and (∗) 12:1. The insert figure is the α-helical percentage of [1−44]apoA-I on the basis of θ_{222} as a function of the initial DMPC:[1−44]apoA-I (w/w) ratio. (B) Negative staining EM image at 45× magnification of the DMPC:[1−44]apoA-I (w/w) 6:1 simple mixture. The samples contained 0.1 mg/mL [1−44]apoA-I and 0.01 M phosphate.

maximum helix content above 7.5:1 (w/w) DMPC:[1−44]-apoA-I. The apparent maximum α-helical content for [1−44]apoA-I in DMPC is ∼45% (the insert to Figure 2A), ∼15% more than that in BOG, but similar to that in SDS. As shown in Figure 2B for the 6:1 (w/w) DMPC:[1−44]apoA-I mixture, negative staining electron microscopy showed many rouleaux of DMPC/[1−44]apoA-I complexes. The thinnest complexes, marked in circles, had a thickness of ∼50 Å, typical of a single phospholipid bilayer. However, there are many particles of ∼100 Å double bilayer thickness individually, at the end, or in the middle of the rouleaux. Those marked with squares probably represent flattened vesicles. The size distribution ranges from 150 to 350 Å in diameter, with a peak at 260 Å. Simple mixtures at other ratios showed similar observations.

(A) Complex Separation by Density Gradient Ultracentrifugation. To further characterize the complexes formed after DMPC/[1−44]apoA-I suspension clearance, DMPC/[1−44]apoA-I complexes were separated by density gradient ultracentrifugation and then visualized by EM. The same eight initial ratios of DMPC:[1−44]apoA-I were studied. Figure 3A shows the lipid distribution, and Figure 3B shows the peptide distribution in the density gradient. Only three initial ratios, 1:1, 2:1, and 3:1, and DMPC alone are shown for clarity. Lipid and peptide peaks for all other initial ratios

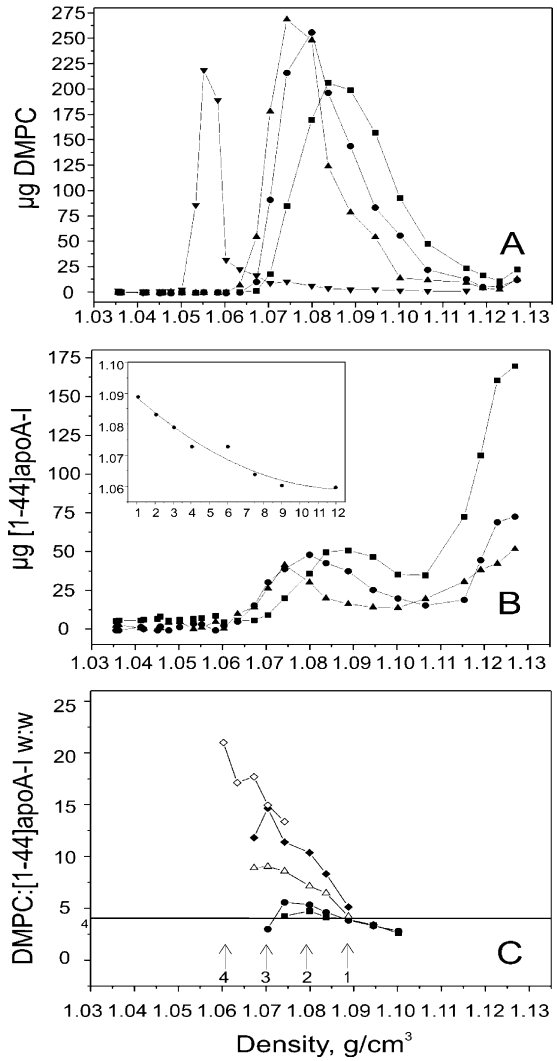

FIGURE 3: Density gradient ultracentrifugation of [1−44]apoA-I/DMPC mixtures at different initial DMPC:[1−44]apoA-I (w/w) ratios. (A) DMPC distribution in the density gradient. Three of the eight ratios are shown for clarity: (■) initial 1:1, (●) initial 2:1, (▲) initial 3:1, and (▼) DMPC alone. (B) The corresponding peptide distribution in the density gradient. Symbols are the same as in (A). The insert figure is the density of the peak fraction as a function of the initial DMPC:[1−44]apoA-I (w/w) ratio. (C) DMPC:[1−44]apoA-I (w/w) ratio for each fraction that contains the complex as a function of density. Four of the eight samples are shown: (■) initial 1:1, (●) initial 2:1, (△) initial 4:1, (◆) initial 6:1, and (◇) initial 12:1. The arrows show the positions of peak fractions: (1) 1:1; (2) 2:1; (3) 4:1 and 6:1; (4) 12:1.

fall between those for the 3:1 ratio and DMPC alone. In all cases, the lipid peak fraction corresponds to the peptide peak fraction. All DMPC, together with most peptide, was enriched at a higher density range than that for free lipid, covering ∼3−5 fractions out of 25 in total. However, there was always some free peptide at the bottom of the centrifuge tube, even in 12:1 samples. As shown in the insert to Figure 3B, as the lipid amount increased in the initial ratios from 1:1 to 12:1, the density of the peak fraction decreased from ∼1.09 g/cm^3 (typical of discoidal complexes formed with apoA-I) to ∼1.06 g/cm^3, the free lipid density.

Weight ratios, derived from panels A and B of Figure 3, for those fractions containing complexes are shown in Figure 3C. For the initial 1:1 ratio, uniform ∼4:1 weight ratio complexes were formed. For the other samples with higher

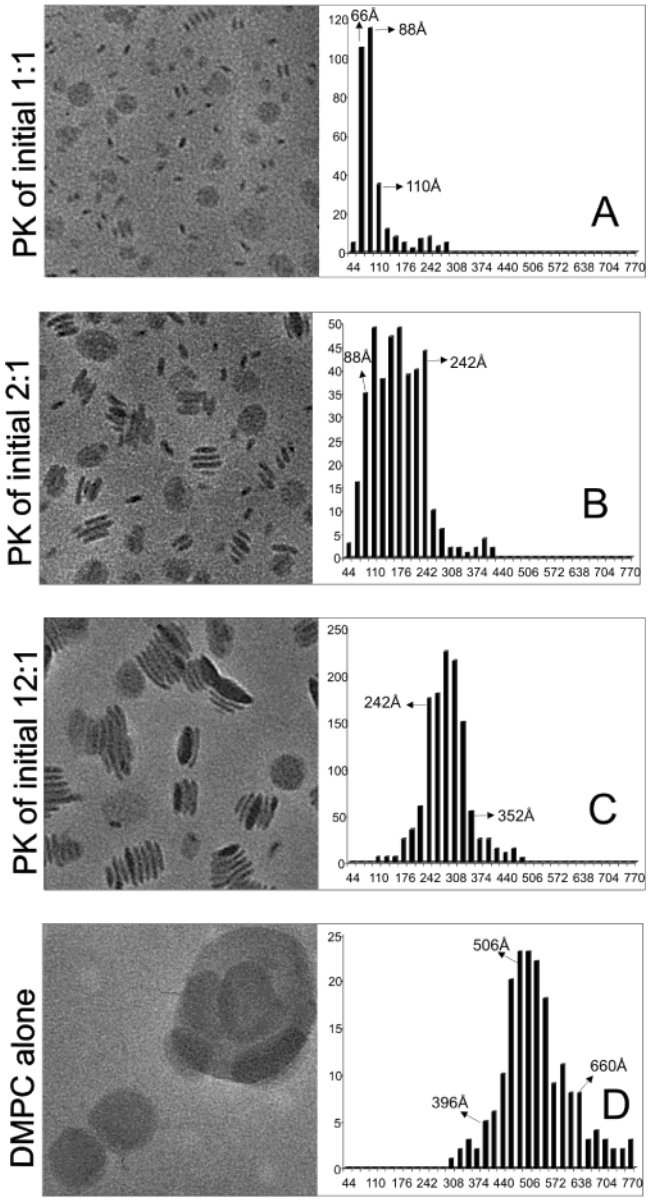

FIGURE 4: Negative staining EM images and size distribution of the peak fraction for various initial DMPC:[1−44]apoA-I (w/w) samples: (A) 1:1, (B) 2:1, (C) 12:1, and (D) DMPC alone.

initial DMPC:[1−44]apoA-I ratios, heterogeneous weight ratio complexes were observed. In all cases, the peak ratio is greater than the initial ratio, and higher initial DMPC:[1−44]apoA-I ratio complexes have higher DMPC:[1−44]-apoA-I ratio at the peak fraction. For instance, for an initial 1:1 ratio, the peak fraction has a ratio of ∼4:1 by weight (30:1 M), and at an initial 4:1 ratio, the peak fraction has a weight ratio of ∼9:1 (65:1 M). At and above an initial 7.5:1 ratio, the DMPC:[1−44]apoA-I ratio in the peak reaches its maximum, which is ∼20:1 by weight and ∼150:1 M.

(B) Complex Visualization by EM. After density gradient ultracentrifuge separation, four to five fractions encompassing the peak for each sample were visualized individually by EM. The left panel of Figure 4 shows micrographs of representative peak fractions of three initial ratio samples and DMPC vesicles alone. The right panel of Figure 4 shows the corresponding size distributions. Two distinct types of complexes, disks and vesicles, were observed. Figure 4A shows the peak aliquot at ∼1.1 g/cm^3 for the initial ratio

DMPC:[1−44]apoA-I (w/w) 1:1. The particles are ∼50 Å in thickness, typical of a single phospholipid bilayer, and ∼70 to ∼110 Å in length. They are typical of disks stacked in rouleaux, singly on-edge and en face. The predominant size is ∼100 Å. Figure 4B shows the 2:1 peak aliquot at 1.085 g/cm^3. Both small (∼100 Å) and larger (up to ∼250 Å) particles are present. Many particles are ∼100 Å thick, typical of two phospholipid bilayers. Some of them show the clear center line of collapsed vesicles. Partially collapsed vesicles and larger face on particles are apparent. Thus, the peak fraction is a mixture of both disks and vesicles, with a wide range of diameters from 90 to 250 Å. For the 2:1 weight ratio, the fraction at higher density had more disks. This was also the case for all other ratios. However, discoidal complexes appeared more rarely as the lipid amount increased. For initial ratios at and below DMPC:[1−44]apoA-I (w/w) 6:1, disks were observed in aliquots at ∼1.1 g/cm^3, while vesicles were predominant in aliquots with density lower than 1.08 g/cm^3. Figure 4C shows the 12:1 weight ratio peak aliquot at ∼1.07 g/cm^3. The predominant size is from ∼260 to ∼380 Å with a mean of ∼300 Å. Collapsed vesicles with double bilayer thickness and ruptured vesicles with single bilayer thickness are present. The vesicle morphology is consistent with the vesicle density of the fraction. Figure 4D shows DMPC vesicles themselves. Two size populations for DMPC vesicles were observed: individually en face with diameter <800 Å and collapsed liposomes with diameter >2000 Å. For the smaller population, the predominant diameter is ∼500 Å. The diameter distribution in Figure 4D is for the smaller measurable population. As shown in the right panel of Figure 4, as the initial lipid:peptide ratio in the sample increases, the predominant size for each peak fraction increases from ∼100 to ∼400 Å, which overlaps with the lower limit of DMPC vesicles themselves. Vesicular complexes have various sizes from 200 to 400 Å, depending on the initial lipid:peptide ratio.

DISCUSSION

Conformation of [1−44]ApoA-I in Solution. [1−44]-ApoA-I is unstructured in aqueous solution (Figure 1A). In contrast to apoA-I, which is self-associated above 0.1 mg/mL, [1−44]apoA-I does not self-associate, even up to 0.5 mg/mL. Considering that [1−44]apoA-I is ∼5 times shorter than apoA-I, at 0.5 mg/mL, the molar concentration of [1−44]apoA-I is ∼25 times higher than the self-association threshold point of the whole A-I molecule.

In the nonionic detergent BOG (Figure 1B), the helical content in [1−44]apoA-I increases in a concentration-dependent manner and then reaches the equilibrium. This is also the case in the presence of SDS, an ionic detergent, TMAO, a protein structure inducer (*29*), and TFE, a helix inducer (Table 1). The maximum α-helix content of [1−44]-apoA-I was obtained in BOG and SDS above their CMC. The maximum percent of α-helix for [1−44]apoA-I at 25 °C is ∼28% in BOG, ∼39% in TMAO, ∼42% in SDS, and ∼45% in TFE. Thus, the maximum inducible helical content for [1−44]apoA-I in aqueous solution is still ∼15% less than the predicted G* helix (*18*) encompassing residues 8−33 (60%).

Thermal unfolding and refolding of [1−44]apoA-I in BOG is reversible from 5 to 95 °C (Figure 1C). In the presence of 0.8% or 1.0% BOG, [1−44]apoA-I at 25 °C undergoes apparent unfolding both on heating and on cooling. However, the CMC of BOG increases as the temperature decreases (*30*), and on cooling below ∼20 °C BOG micelles dissociate, resulting in the loss of helical structure for [1−44]apoA-I in 0.8% and 0.9% BOG. At higher BOG concentrations (1.2% and 3.0%), the micelle is stable at low temperature (<25 °C) and the peptide helical conformation is maintained. On heating from 25 °C, the peptide unfolds although the BOG micelles may still exist. [1−44]ApoA-I reaches the maximum helical structure of ∼30% in 3.0% BOG at 0 °C.

In SDS, TMAO, and TFE, thermal unfolding and refolding of [1−44]apoA-I are also reversible. However, in contrast to [1−44]apoA-I in BOG, SDS, and TFE, where the CD data do not exhibit clear baselines at both high and low temperature (although there is a tendency to reach them), the CD data for [1−44]apoA-I in 6 M TMAO show two clear baselines at both high and low temperature. This suggests that the thermal unfolding and refolding of [1−44]apoA-I is more cooperative in TMAO than in BOG, SDS, and TFE. In addition, the midpoint of the thermal unfolding (T_m) for [1−44]apoA-I in TMAO is ∼25 °C compared ∼50 °C for [1−44]apoA-I in BOG/SDS/TFE.

[1−44]ApoA-I Binds to Lipid and Forms Discoidal Complexes. [1−44]ApoA-I solubilized DMPC liposomes into a heterogeneous population of vesicular structures with a density range from ∼1.085 to ∼1.07 g/cm^3, as well as small discoidal complexes with a diameter of ∼100 Å and a density of ∼1.1 g/cm^3. Both the size and the density of the discoidal complexes are similar to those of the discoidal HDL formed from A-I and phosphatidylcholine (*31*). According to the density gradient ultracentrifugation data, as the initial DMPC:[1−44]apoA-I (w/w) ratio increased from 1:1 to 12:1, the peak fraction density decreased from ∼1.1 g/cm^3, typical of the density of DMPC/A-I disks, to ∼1.07 g/cm^3, close to the lipid density (insert to Figure 3B). Data from EM are consistent with that from the density gradient. Discoidal complexes (Figure 4A), with ∼100 Å diameter at ∼1.1 g/cm^3 fraction, were formed when a large excess of peptide was present in the mixture, at the initial DMPC:[1−44]apoA-I 1:1 (w/w) ratio. For an initial ratio 2:1 sample, complexes were a mixture of both disks and vesicles (Figure 4B). For initial ratios higher than 3:1, vesicles are predominant (Figure 4C), with sizes from ∼200 to ∼500 Å, the predominant size of DMPC vesicles. Thus, this study provides strong and direct evidence that the exon 3 encoded N-terminal region of human apoA-I binds to lipid to form both discoidal complexes and vesicular structures with peptide bound.

[1−44]ApoA-I Has Moderate Lipid Binding Affinity. The percentage of bound [1−44]apoA-I increases with increasing lipid amount and becomes constant at DMPC:[1−44]-apoA-I (w/w) ratios higher than 7.5:1 (Figure 5A). This equilibrium may be described by the equation (*32*):

$$K_D = (N[PC] - [P_B])[P_F]/[P_B]$$

where $[P_F]$ is the free protein concentration, [PC] is the lipid concentration, and $[P_B]$ is the lipid-bound protein concentration. This equation can be linearized to (*33*)

$$[P_F] = N[PC][P_F]/[P_B] - K_D$$

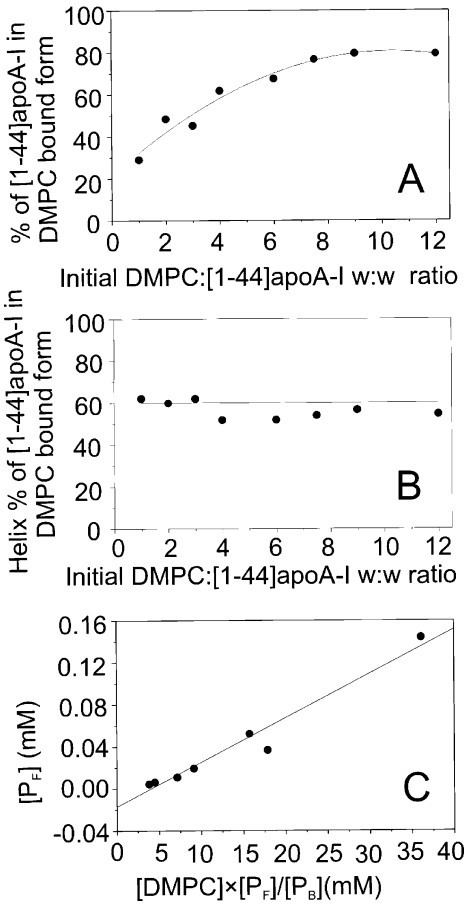

FIGURE 5: (A) Percentage of lipid-bound [1−44]apoA-I as a function of the initial DMPC:[1−44]apoA-I (w/w) ratio derived from data in Figure 3. The solid curve is the polynomial regression fitting curve of the order 2, $R^2 = 0.95$. (B) Calculated helical content for [1−44]apoA-I in lipid-bound form as a function of the initial lipid:peptide (w/w) ratio. Data are calculated from the combination helical percentages in Figure 2A and the bound percentages in panel A. The solid line is the 60% marker. (C) Linearized plots of the eight ratios studied from the density gradient according to the equation $[P_F] = (N[DMPC][P_F]/[P_B]) - K_D$. The solid line represents the linear fitting of the data, $R^2 = 0.96$.

Figure 5C shows the linearized plots for the eight ratios studied, derived from the density gradient data. The data set fits the linear plot well ($R^2 = 0.96$), which supports the analysis of the [1−44]apoA-I/DMPC interaction by this model. The K_D for [1−44]apoA-I binding to DMPC is ∼0.02 mM, which is about 20-fold higher than that determined for apoA-I−lecithin interaction (*33*) and indicates moderate lipid binding affinity for [1−44]apoA-I.

The low lipid affinity of [1−44]apoA-I was suggested by its sequence and the predicted amphipathic G* helix (residues 8−33) (*19*). The simple G-type helix is the typical helix conformation of globular proteins, with a random charge distribution in the polar face (*19*). In contrast to the G helix, a typical lipid binding, type A, amphipathic helix as found in the exon 4 encoded region of apoA-I has a regular positive/negative charge distribution in the polar face. Thus, based on charge distribution, the G* helix in [1−44]apoA-I, with a random charge distribution in the polar face, was thought not to interact with lipid (*19*). However, the G* helix has a larger hydrophobic face than that of the typical G helix. The large hydrophobic face may give the peptide the ability to interact with lipid but not with the high affinity of the type A helix.

Because of its moderate lipid binding affinity, [1−44]-apoA-I only forms discoidal complexes under conditions of excess peptide although the peptide can solubilize DMPC and form vesicular complexes over a wide range of lipid-to-peptide ratios. For example, at an initial weight ratio of 1:1 DMPC:[1−44]apoA-I the discoidal complexes isolated from the density gradient have a ratio of 4:1 DMPC:[1−44]apoA-I. An initial weight ratio of 4:1 results in the formation of a higher 9:1 ratio vesicular complex. This is in contrast to apoA-I with higher lipid binding affinity that forms discrete stoichiometric complexes with phospholipids independent of the initial lipid-to-protein ratio (*33*). For the vesicular complexes, the peptide must be responsible for the disruption of the multilamellar DMPC and stabilization of the vesicles. The larger hydrophobic face of the G* helix probably associates with the lipid surface and thus stabilizes the vesicular complexes. Although it is possible that the peptides specifically interact with each other, to form a well-defined structure that then interacts with lipid, since [1−44]-apoA-I does not self-associate in solution, this is unlikely.

Helical Content for [1−44]ApoA-I in Lipid-Bound Form. The CD spectra in Figure 2A represent the weighted combination of the CD signal for both lipid-free and lipid-bound [1−44]apoA-I. Using the data for the amount of [1−44]apoA-I bound versus free derived from the density gradient (Figure 5A), we calculated the percentage of α-helix (% α) for the lipid-bound form. At all of the eight ratios studied, the helical content for [1−44]apoA-I in lipid-bound form is ∼60% (Figure 5B). Conversely, assuming there is 60% helical structure in lipid-bound [1−44]apoA-I and combining the percentage of lipid-bound peptide, the apparent far-UV CD helical signal for each ratio sample was predicted and compared to that determined from θ_{222} (25 °C). Consistency between the two data sets demonstrated that the apparent CD signal did reflect the lipid-bound percentage of [1−44]apoA-I at each ratio. It is dramatic that ∼60% of this exon 3 encoded region becomes α-helix from random coil on lipid binding. The α-helical content of [1−44]apoA-I in the lipid-bound form corresponds to the percentage predicted by the G* helix (residues 8−33) (*18*) and is also consistent with the NMR assignments (residues 8−32) obtained in 280 mM SDS solution (*9*, *10*).

The well-documented increase in helicity of apoA-I on lipid association may, at least in part, result from the helix formation in this N-terminal region. ApoA-I in which the N-terminal region has been deleted, Δ(1−43)A-I, has been suggested to adopt the helical content of the lipid-bound form (*34*). However, studies of Δ(1−41)A-I have suggested that the deletion of this region results in the disruption of helical conformation (*23*). Also, studies of internal deletion mutants have suggested that the segment, residues 121−144, may be involved in the helix formation on lipid binding (*27*). Thus, a precise delineation of the regions of apoA-I that change conformation on lipid binding remains to be achieved.

It is generally thought that protein conformation in BOG micelles represents the lipid-bound form (*35*, *36*). However, from the far-UV CD study of this N-terminal peptide, it is clear that this assumption may not always be valid. The maximum helix for [1−44]apoA-I in BOG is ∼30%, half of that in DMPC. This suggests that upon lipid binding the

peptide adopts a conformation different from that in BOG solution. Similarly, NMR data obtained in SDS may represent a conformation different from that of the phospholipid-bound form.

[1−44]ApoA-I and DMPC Disk Formation. The DMPC/[1−44]apoA-I disks were formed spontaneously by simply mixing the peptide with DMPC liposomes. These DMPC/[1−44]apoA-I disks are stable, although only in the presence of excess peptide. Since the initial 1:1 ratio peak fraction was almost pure disks, we assume that the composition of peptide and lipid in the peak fraction represents that in the particles with a mean size of ∼100 Å (Figure 4A). The molar DMPC:[1−44]apoA-I ratio at the peak fraction of the initial 1:1 weight ratio is ∼30:1, and the composition of the 100 Å discoidal complex is ∼5 [1−44]apoA-I and ∼150 DMPC per disk. The helix length of five [1−44]apoA-I molecules with ∼60% α-helix is just long enough to wrap around the DMPC bilayer disk once. Thus, in contrast to the current models for apoA-I-stabilized disks, where two molecules of the protein are thought to form a double belt stabilizing the disk edge, disk formation and stabilization by the small N-terminal peptide are achieved with a single belt.

In conclusion, the first 44 residues ([1−44]apoA-I) of human apoA-I have a moderate lipid binding affinity and can form both disks in the presence of excess peptide and vesicles of various sizes, over a wide range of the peptide:lipid ratios. [1−44]ApoA-I is unstructured in the lipid-free state and becomes ∼60% helix on interaction with phospholipid, irrespective of the formation of discoidal or vesicular complexes. This suggests that although apoA-I undergoes dramatically tertiary conformational changes, the helical content of the N-terminal region remains stable during transformation of nascent discoidal HDL to mature spherical HDL.

ACKNOWLEDGMENT

We are grateful to Donald Gantz for help with the EM techniques and to Dr. Yiling Fang for help with the CD and lipid binding characterization techniques. We thank Cheryl England and Michael Gigliotti for general assistance.

REFERENCES

1. Forte, T. M., and McCall, M. R. (1994) The role of apolipoprotein A-I-containing lipoproteins in atherosclerosis, *Curr. Opin. Lipidol. 5*, 354−364.
2. Walldius, G., and Jungner, I. (2004) Apolipoprotein B and apolipoprotein A-I: risk indicators of coronary heart disease and targets for lipid-modifying therapy, *J. Intern. Med. 255*, 188−205.
3. Fielding, C. J., and Fielding, P. E. (1995) Molecular physiology of reverse cholesterol transport, *J. Lipid Res. 36*, 211−228.
4. Rye, K. A., and Barter, P. J. (2004) Formation and metabolism of prebeta-migrating, lipid-poor apolipoprotein A-I, *Arterioscler., Thromb., Vasc. Biol. 24*, 421−428.
5. Tall, A. R. (1998) An overview of reverse cholesterol transport, *Eur. Heart J. 19* (Suppl. A), A31−A35.
6. Marcel, Y. L., and Kiss, R. S. (2003) Structure−function relationships of apolipoprotein A-I: a flexible protein with dynamic lipid associations, *Curr. Opin. Lipidol. 14*, 151−157.
7. Nolte, R. T., and Atkinson, D. (1992) Conformational analysis of apolipoprotein A-I and E−3 based on primary sequence and circular dichroism, *Biophys. J. 63*, 1221−1239.
8. Borhani, D. W., Rogers, D. P., Engler, J. A., and Brouillette, C. G. (1997) Crystal structure of truncated human apolipoprotein A-I suggests a lipid-bound conformation, *Proc. Natl. Acad. Sci. U.S.A. 94*, 12291−12296.
9. Okon, M., Frank, P. G., Marcel, Y. L., and Cushley, R. J. (2001) Secondary structure of human apolipoprotein A-I(1−186) in lipid-mimetic solution, *FEBS Lett. 487*, 390−396.
10. Okon, M., Frank, P. G., Marcel, Y. L., and Cushley, R. J. (2002) Heteronuclear NMR studies of human serum apolipoprotein A-I. Part I. Secondary structure in lipid-mimetic solution, *FEBS Lett. 517*, 139−143.
11. Scott, B. R., McManus, D. C., Franklin, V., McKenzie, A. G., Neville, T., Sparks, D. L., and Marcel, Y. L. (2001) The N-terminal globular domain and the first class A amphipathic helix of apolipoprotein A-I are important for lecithin:cholesterol acyltransferase activation and the maturation of high density lipoprotein in vivo, *J. Biol. Chem. 276*, 48716−48724.
12. Sorci-Thomas, M. G., Thomas, M., Curtiss, L., and Landrum, M. (2000) Single repeat deletion in ApoA-I blocks cholesterol esterification and results in rapid catabolism of delta6 and wild-type ApoA-I in transgenic mice, *J. Biol. Chem. 275*, 12156−12163.
13. McManus, D. C., Scott, B. R., Frank, P. G., Franklin, V., Schultz, J. R., and Marcel, Y. L. (2000) Distinct central amphipathic alpha-helices in apolipoprotein A-I contribute to the in vivo maturation of high density lipoprotein by either activating lecithin-cholesterol acyltransferase or binding lipids, *J. Biol. Chem. 275*, 5043−5051.
14. Cho, K. H., Durbin, D. M., and Jonas, A. (2001) Role of individual amino acids of apolipoprotein A-I in the activation of lecithin: cholesterol acyltransferase and in HDL rearrangements, *J. Lipid Res. 42*, 379−389.
15. Roosbeek, S., Vanloo, B., Duverger, N., Caster, H., Breyne, J., De Beun, I., Patel, H., Vandekerckhove, J., Shoulders, C., Rosseneu, M., and Peelman, F. (2001) Three arginine residues in apolipoprotein A-I are critical for activation of lecithin:cholesterol acyltransferase, *J. Lipid Res. 42*, 31−40.
16. Reardon, C. A., Kan, H. Y., Cabana, V., Blachowicz, L., Lukens, J. R., Wu, Q., Liadaki, K., Getz, G. S., and Zannis, V. I. (2001) In vivo studies of HDL assembly and metabolism using adenovirus-mediated transfer of ApoA-I mutants in ApoA-I-deficient mice, *Biochemistry 40*, 13670−13680.
17. Frank, P. G., and Marcel, Y. L. (2000) Apolipoprotein A-I: structure−function relationships, *J. Lipid Res. 41*, 853−872.
18. Segrest, J. P., Jones, M. K., De Loof, H., Brouillette, C. G., Venkatachalapathi, Y. V., and Anantharamaiah, G. M. (1992) The amphipathic helix in the exchangeable apolipoproteins: a review of secondary structure and function, *J. Lipid Res. 33*, 141−166.
19. Brouillette, C. G., and Anantharamaiah, G. M. (1995) Structural models of human apolipoprotein A-I, *Biochim. Biophys. Acta 1256*, 103−129.
20. Mishra, V. K., Palgunachari, M. N., Datta, G., Phillips, M. C., Lund-Katz, S., Adeyeye, S. O., Segrest, J. P., and Anantharamaiah, G. M. (1998) Studies of synthetic peptides of human apolipoprotein A-I containing tandem amphipathic alpha-helixes, *Biochemistry 37*, 10313−10324.
21. Tricerri, M. A., Behling Agree, A. K., Sanchez, S. A., and Jonas, A. (2000) Characterization of apolipoprotein A-I structure using a cysteine-specific fluorescence probe, *Biochemistry 39*, 14682−14691.
22. Behling Agree, A. K., Tricerri, M. A., Arnvig McGuire, K., Tian, S. M., and Jonas, A. (2002) Folding and stability of the C-terminal half of apolipoprotein A-I examined with a Cys-specific fluorescence probe, *Biochim. Biophys. Acta 1594*, 286−296.
23. Fang, Y., Gursky, O., and Atkinson, D. (2003) Structural studies of N- and C-terminally truncated human apolipoprotein A-I, *Biochemistry 42*, 6881−6890.
24. Gursky, O., and Atkinson, D. (1996) Thermal unfolding of human high-density apolipoprotein A-1: implications for a lipid-free molten globular state, *Proc. Natl. Acad. Sci. U.S.A. 93*, 2991−2995.
25. Lowry, O. H., Rosebrough, N. J., Farr, A. L., and Randall, R. J. (1951) Protein measurement with the Folin Phenol reagent, *J. Biol. Chem. 193*, 265−275.
26. Mao, D., and Wallace, B. A. (1984) Differential light scattering and absorption flattening optical effects are minimal in the circular dichroism spectra of small unilamellar vesicles, *Biochemistry 23*, 2667−2673.
27. Fang, Y., Gursky, O., and Atkinson, D. (2003) Lipid-binding studies of human apolipoprotein A-I and its terminally truncated mutants, *Biochemistry 42*, 13260−13268.
28. Chao, Y., and Atkinson, D. (2003) Conformational studies of a consensus sequence peptide (CSP) and a real sequence peptide (RSP) of apolipoproteins by circular dichroism spectrscopy and

X-ray crystallography, Ph.D. Thesis, Boston University (University Microfilms International Publication AAT 3068030, ISBN: 0-493-87349-X).
29. Baskakov, I., and Bolen, D. W. (1998) Forcing thermodynamically unfolded proteins to fold, *J. Biol. Chem. 273*, 4831−4834.
30. da Graca Miguel, M., Eidelman, O., Ollivon, M., and Walter, A. (1989) Temperature dependence of the vesicle-micelle transition of egg phosphatidylcholine and octyl glucoside, *Biochemistry 28*, 8921−8928.
31. Atkinson, D., and Small, D. M. (1986) Recombinant lipoproteins: implications for structure and assembly of native lipoproteins, *Annu. Rev. Biophys. Biophys. Chem. 15*, 403−456.
32. Yokoyama, S., Fukushima, D., Kupferberg, J. P., Kezdy, F. J., and Kaiser, E. T. (1980) The mechanism of activation of lecithin: cholesterol acyltransferase by apolipoprotein A-I and an amphiphilic peptide, *J. Biol. Chem. 255*, 7333−7339.
33. Derksen, A., and Small, D. M. (1989) Interaction of ApoA-1 and ApoE−3 with triglyceride-phospholipid emulsions containing increasing cholesterol concentrations. Model of triglyceride-rich nascent and remnant lipoproteins, *Biochemistry 28*, 900−906.
34. Rogers, D. P., Brouillette, C. G., Engler, J. A., Tendian, S. W., Roberts, L., Mishra, V. K., Anantharamaiah, G. M., Lund-Katz, S., Phillips, M. C., and Ray, M. J. (1997) Truncation of the amino terminus of human apolipoprotein A-I substantially alters only the lipid-free conformation, *Biochemistry 36*, 288−300.
35. Kumar, M. S., Carson, M., Hussain, M. M., and Murthy, H. M. (2002) Structures of apolipoprotein A-II and a lipid-surrogate complex provide insights into apolipoprotein−lipid interactions, *Biochemistry 41*, 11681−11691.
36. Maulik, P. R., Reed, R. A., Sparrow, D. A., Sparrow, J. T., and Shipley, G. G. (1990) Crystallization and preliminary X-ray diffraction study of synthetic apolipoprotein E fragment (residues 129−169), *J. Biol. Chem. 265*, 490−492.

BI0487894